Silicon (2022) 14:1421–1429
https://doi.org/10.1007/s12633-020-00899-z

ORIGINAL PAPER

# Investigation of Influence of SiN and $SiO_2$ Passivation in Gate Field Plate Double Heterojunction $Al_{0.3}Ga_{0.7}N/GaN/Al_{0.04}Ga_{0.96}N$ High Electron Mobility Transistors

P. Murugapandiyan[1] · D. Nirmal[2] · J. Ajayan[3] · Arathy Varghese[4] · N. Ramkumar[1]

Received: 7 July 2020 / Accepted: 11 December 2020 / Published online: 21 January 2021


## Abstract

This research article reports the operational characteristics of gate field plate double heterojunction (DH) high electron mobility transistors (HEMTs) using SiN ($SiO_2$) passivation techniques. The proposed HEMT exhibits 496 (292) V breakdown voltage ($V_{BR}$) for $L_G$ (gate-length) = 0.25 μm, $L_{GD}$ (drain-gate distance) = 3.2 μm and 1 μm field plate length HEMT. The n + GaN source/drain regions with SiN ($SiO_2$) passivation AlGaN/GaN/AlGaN HEMT delivered 1.4 (1.3) A/mm peak drain current density ($I_{ds}$), 540 (550) mS/mm $g_m$ (transconductance), $f_T/f_{MAX}$ of 54/198 (62/252) GHz, and the sub-threshold drain leakage current of $4 \times 10^{-13}$ ($1 \times 10^{-11}$) A/mm. The high Johnson figure of merit (JFoM = $f_T \times V_{BR}$) of 28.76 (19.27) THz.V and excellent $V_{BR} \times f_{MAX}$ product of 90.27 (73.29) THz.V demonstrates the great potential of the optimized gate field plate DH-HEMTs structure for U and V band high power microwave electronics.

**Keywords** Field plate · HEMT · Johnson figure of merit · Microwave applications · Passivation

## 1 Introduction

AlGaN/GaN HEMTs had proven their capability for high power microwave and switching application domains owing to their outstanding material characteristics such as excellent saturation electron velocity (~$2 \times 10^7$ cm/s), low ON-resistance, large breakdown electric field of GaN (3 MV/cm), and inherent high electron mobility of 1500–2000 $cm^2$/V.s that can be achieved even without intentional doping [1–5].

✉ D. Nirmal
dnirmalphd@gmail.com

P. Murugapandiyan
murugavlsi@gmail.com

1 Department of Electronics and Communication Engineering, Anil Neerukonda Institute of Technology & Sciences, Visakhapatnam, Andhra Pradesh, India

2 Department of Electronics and Communication Engineering, Karunya Institute of Technology and Sciences, Coimbatore, Tamilnadu, India

3 Department of Electronics and Communication Engineering, SR University, Warangal, Telangana, India

4 School of Engineering, Cardiff University, Cardiff, Wales, UK

At high drain bias, HEMTs experiences a high electric-field intensity near the drain edge of the gate. This non-uniform electric field distribution is regarded as the reason for the early breakdown seen in HEMTs as this leads to increased leakage current and current collapse [6–11]. Current collapse is the phenomenon that occurs when a high electric field or drain voltage of the device. The electrons get trapped in the free surface states, causing virtual gating which results in collapsing of the drain current. It becomes essential to scale-down the device dimensions to enable high-speed operation, this may lead to increased current collapse because of the shorter gate-drain spacing. To improve the breakdown characteristics of the HEMT and to avoid the current collapse phenomena, it is required to suppress the field intensity between the gate to drain access region. Maintaining a uniform electric field in the 2DEG region, several optimization techniques are adopted such as drain field plate, gate field plate, source field plate, discrete field plate, slant field plate, and high-*k* passivation techniques. However, simultaneous improvement in the breakdown voltage and the cut-off frequency is yet another key challenge to the device researchers. Management of electric field in the 2DEG region becomes even more critical for nanometer scaled devices. These problems limit the scaling of high power GaN HEMTs for millimeter-wave electronics [12–26].

A Field plated gate structure enhances the power performances by simultaneous reduction of current collapse and enhancement of the breakdown voltage [27–30]. Suboptimal breakdown at 65 V is reported in a 0.2 μm gate length field plate gate AlGaN/GaN HEMT with $f_T/f_{MAX}$ of 60/100 GHz [2]. 0.1 μm gate AlGaN/GaN HEMT device as it exhibited a 176 V breakdown voltage for $L_{GD} = 2$ μm and $f_T/f_{MAX}$ of 50/120 GHz [7]. Further, a 0.6 μm channel length based field plate gate AlGaN/GaN HEMT exhibited $f_T/f_{MAX}$ of 19/50 GHz and 82 V OFF-state $V_{BR}$ for $L_{GD} = 2.8$ μm [12]. The impact of passivation thickness and permittivity on the breakdown voltage of the AlGaN/GaN HEMTs has been studied extensively [30–36] and the high-*k* passivation techniques improved the $V_{BR}$ of the device significantly. However, the high *k*-passivation limits the operating frequency of the HEMT due to an increase in device intrinsic capacitances ($C_{GS}$ and $C_{GD}$). Because, the $f_T$ (cut-off frequency) and $f_{MAX}$ (maximum oscillation frequency) of the HEMTs are limited by the device intrinsic capacitances ($C_{GS} + C_{GD}$) and contact resistances ($R_S$ and $R_D$) [14–16]. Another important issue in the GaN-based HEMT is maximum current density is still below the theoretical value ($I_{DS} \propto q.n_s.v_{sat}$). Where, q is electron charge, $n_s$ represents sheet charge density in the channel, and $v_{sat}$ represents saturation velocity of the carrier. Therefore, proper device design is required for attaining together high drain current density, $f_T/f_{MAX}$ and $V_{BR}$.

In this work, we present gate field plate $Al_{0.3}Ga_{0.7}N$/GaN HEMT with $Al_{0.04}Ga_{0.96}N$ as a buffer region. The access resistance in the device is reduced through the use of n + GaN ohmic source/drain (S/D) regions and the device surface passivation (low permittivity) along with field plate flattening the electric field distribution. The $Al_{0.04}Ga_{0.96}N$ blocking layer introduced as a performance booster in the proposed device design helps in exemplary confinement of charge carriers in the device channel, leading to a considerable suppression of the buffer leakage, sub-threshold drain leakage, and enhanced two-dimensional electron gas (2DEG). The device operational characteristics are analyzed using a thick 0.5 μm SiN and $SiO_2$ passivation techniques.

## 2 Device Architecture and Simulation Models

The proposed device architecture is shown in Fig. 1. The TCAD simulation energy band diagram of double heterostructures DH-HEMT (AlGaN/GaN/AlGaN) and conventional HEMT (AlGaN/GaN) are depicted in Figs. 2 and 3 respectively. The proposed HEMT constitute of a 20 nm $Al_{0.3}Ga_{0.7}N$ barrier, 65 nm GaN channel, and 750 nm $Al_{0.04}Ga_{0.96}N$ buffer (back-barrier). The device surface is passivated by 0.5 μm thickness (t) of $SiN/SiO_2$ and SiC used as substrate for good thermal conductivity. A 100 nm AlN layer sandwiched between buffer and substrate for low lattice mismatch. The thickness of the passivation and permittivity majorly impacts on the breakdown characteristics of the HEMT by influencing the distribution of electric field in the device access region [36]. The $L_{GS}$ (gate to source spacing), $L_G$, $L_{FP}$ (field plate length), gate width (W), and $L_{GD}$ of the proposed unsymmetrical HEMT are 0.45 μm, 0.25 μm, 1 μm, 0.6 μm, and 3.2 μm respectively.

The gate-drain distance is intentionally kept larger than the source-gate distance to ensure device performance in terms of reduced source resistance and enhanced device reliability. The drain and source areas are obtained by 100 nm heavily doped (Si ~ $1 \times 10^{16}$ /$cm^3$) n + GaN for low contact resistances [37]. The introduction of a low Al-content $Al_{0.04}Ga_{0.96}N$ back-barrier (blocking layer) provides more effective electron confinement in the GaN channel as shown in Fig. 2. Lower Al content in the buffer region is desirable as it aids in avoiding excessive stress in the GaN channel and also avoids the interface roughness, which impacts the 2DEG mobility [19]. The $Al_{0.04}Ga_{0.96}N$ blocking layer introduces the conduction band offset and negative polarization-charge at the AlGaN/GaN interface, which increase the carrier confinement. The proposed combination of field plate gate in double heterojunctions HEMTs (DH-HEMTs) suppresses the drain leakage and buffer leakage in the device thereby enhancing the device breakdown voltage ($V_{BR}$). The Schottky contact for the gate electrode is realized by setting the metal work function at 5.2 eV.

The Silvaco ATLAS simulator tool is employed for the simulation of the device that considers both electron and holes for analyzing the I-V characterization of the device using the Poisson and continuity equations. To investigate the $Al_{0.3}Ga_{0.7}N/In_{0.1}Ga_{0.9}N/GaN/Al_{0.04}Ga_{0.96}N$ HEMT DC and RF characteristics, the essential transport, material dependent physics, recombination, and generation models are adopted in the TCAD simulation. The Drift-Diffusion transport model, nitride specific low and high field mobility models, and SRH (Shockley–Read–Hall recombination). The breakdown analysis of the device has been performed by incorporating the temperature-dependent impact ionization Selberherr models [20]. The list of material parameters for numerical simulation is shown in Table 1. The defects or traps in the bandgap of semiconductors lead to phonon transitions. The SRH recombination is modeled as follows [20]:

$$R_{SRH} = \frac{pn - n_{ie}^2}{TAUN0\left[n + n_{ie}\exp\left(\frac{ETRAP}{kT_L}\right)\right] + TAUP0\left[p + n_{ie}\exp\left(\frac{ETRAP}{kT_L}\right)\right]} \quad (1)$$

Where ETRAP represent trap energy level, $T_L$ is the lattice temperature, TAUNO and TAUPO accounts fro carrier life time.

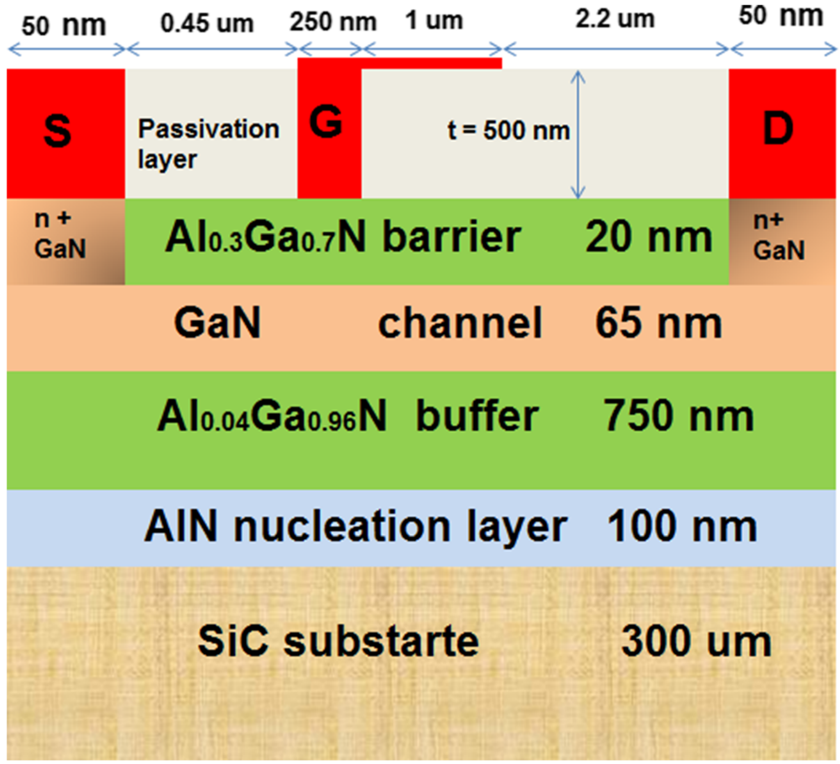


**Fig. 1** Architecture of proposed gate field plate DH-HEMT

The Selberherr impact ionization model is considered in simulation profile, which can be expressed as [20].

$$\alpha_n = \mathrm{ANexp}\left[-\left(\frac{\mathrm{BN}}{\mathrm{E}}\right)^{\mathrm{BETAN}}\right]\alpha_n$$
$$= \mathrm{ANexp}\left[-\left(\frac{\mathrm{BN}}{\mathrm{E}}\right)^{\mathrm{BETAN}}\right] \quad (2)$$

$$\alpha_n = \mathrm{ANexp}\left[-\left(\frac{\mathrm{BN}}{\mathrm{E}}\right)^{\mathrm{BETAN}}\right]\alpha_n$$
$$= \mathrm{ANexp}\left[-\left(\frac{\mathrm{BN}}{\mathrm{E}}\right)^{\mathrm{BETAN}}\right] \quad (3)$$

$\alpha_n = \mathrm{ANexp}\left[-\left(\frac{\mathrm{BN}}{\mathrm{E}}\right)^{\mathrm{BETAN}}\right]$ Here, $\alpha_n$ and $\alpha_p$ are electron and hole ionization rates respectively. AN, BN, AP,

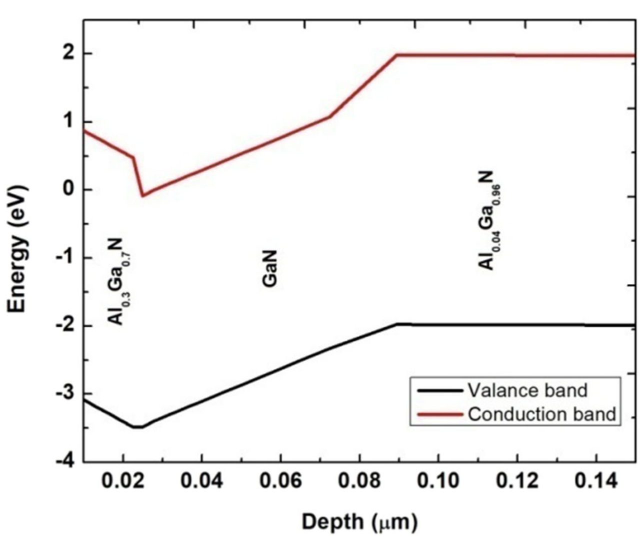


**Fig. 2** Energy band discontinuity of DH-HEMT

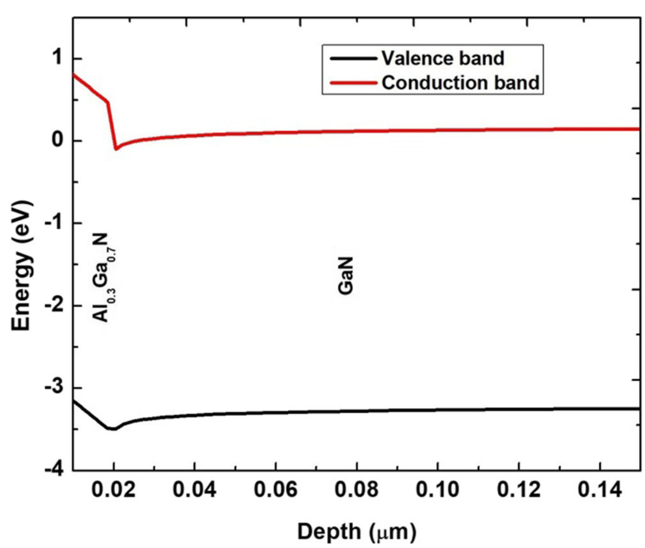


**Fig. 3** Energy band discontinuity of conventional HEMT

**Table 1** Parameters used in TCAD Simulation

| Parameter | Unit | GaN | AlGaN |
|---|---|---|---|
| The Semiconductor band gap ($E_g$) | eV | 3.4 | 3.96 |
| Relative permittivity ($\mathcal{E}_r$) | – | 9.5 | 9.5 |
| High field electron mobility (μ) | $cm^2/V.s$ | GANSAT Mobility model [20] | |
| Low field electron mobility (μ) | $cm^2/V.s$ | 1460 | 300 |
| Electron saturation velocity | cm/s | $2 \times 10^7$ | $1.12 \times 10^7$ |
| Hole saturation velocity | cm/s | $1.9 \times 10^7$ | $1.0 \times 10^6$ |
| Electron affinity | eV | 4 | 3.82 |
| SRH lifetime | – | $1.0 \times 10^7$ | $1.0 \times 10^7$ |
| DOS: Conduction band ($\times 10^{18}$) | $cm^{-3}$ | 1.07 | 2.07 |
| DOS: Valence band ($\times 10^{19}$) | $cm^{-3}$ | 1.16 | 1.16 |

BP, BETAN and BETAP are the fitting parameters in the model.

$$P_{RF} = \frac{I_{MAX}(V_{BR} - V_{KNEE})}{8} \quad (4)$$

The impact ionization process is the major factor that leads to breakdown of a HEMT device [38–40]. In order to improve the accuracy of breakdown simulation, trap effects have been included in the Poisson equation which is expressed as [41]:

$$\Delta\varepsilon\Delta\varphi = -q(p - n + N_D - N_A) - \rho_{trap} \quad (5)$$

Where $\rho_{trap}$, $N_A$, $N_D$, p, n, φ and ε represents density of charge traps, ionized acceptor concentration, ionized donor concentration, hole concentration, electron concentration, electrostatic potential and permittivity respectively.

## 3 Results and Discussions

2-DEG density and carrier mobility of $1.21 \times 10^{13}$ $cm^{-2}$ and 1260 $cm^2$/V-s respectively are extracted from the TCAD simulation of the proposed device. The enhanced electron confinement is mainly due to the induction of negatively polarized charges at the $Al_{0.04}Ga_{0.96}N$/GaN interface, rather than the discontinuity present in the conduction band as seen in Fig. 2 due to the conduction band offsets. These charges present at the interface at thermal equilibrium introduce a significant bending of the energy bands. This band bending leads to the development of a very huge barrier whose height/offset increases with the Al concentration of the back-barrier along with the HEMT channel width. The passivation layer thickness (t), the permittivity of the passivation dielectric ($\varepsilon_i$), field plate length ($L_{FP}$), and gate to drain distance ($L_{GD}$) are influences the field distribution along the channel [36]. Despite the high breakdown voltage for high-*k* passivation HEMT, device cut-off frequency is reduced due to an increase in intrinsic parasitic capacitances ($C_{GD}$ and $C_{GS}$). In this work, the device characteristics are analyzed using a low-*k* SiN ($\varepsilon_i \sim 7.5$) and $SiO_2$ ($\varepsilon_i \sim 3.9$) passivation techniques.

From the basic RF output power Eq. (4) of a power amplifier, the high $V_{BR}$ and high current density of the HEMT are essential parameter for high power output and high power-added efficiency. In general, as the gate-drain distance ($L_{GD}$) shortened in nano-scale HEMT, results in peak electric field near the drain edge of the gate, which leads to virtual gating effects and current collapse phenomena in HEMTs. Additional field plates and passivation techniques improve the breakdown voltage by maintains uniform field distribution in the access area. In the proposed HEMT structure, the gate-drain distance ($L_{GD} = 3.2$ μm) is kept higher than the gate-source distance, and also a thick passivation technique is used to improve the $V_{BR}$.

Figure 4 presents the breakdown voltage curves of 0.25 μm gate length conventional and proposed DH-HEMTs. The proposed device with SiN passivation device surface had shown outstanding breakdown voltage of 496 V and $SiO_2$ passivation HEMT had shown 292 V. The conventional HEMTs with SiN passivation device surface demonstrated a breakdown voltage of 449 V and $SiO_2$ passivation HEMT had shown 220 V.

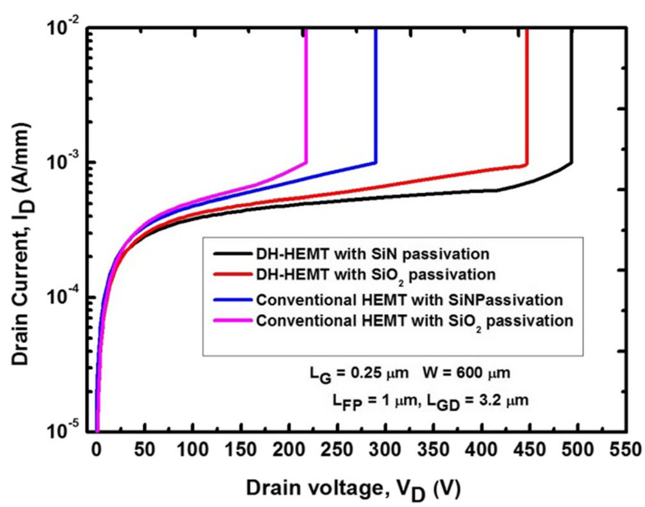


**Fig. 4** Breakdown characteristics

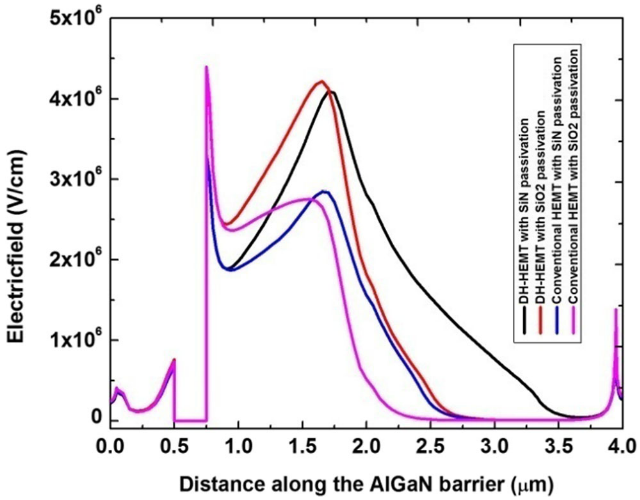


**Fig. 5** Field distribution along the AlGaN barrier

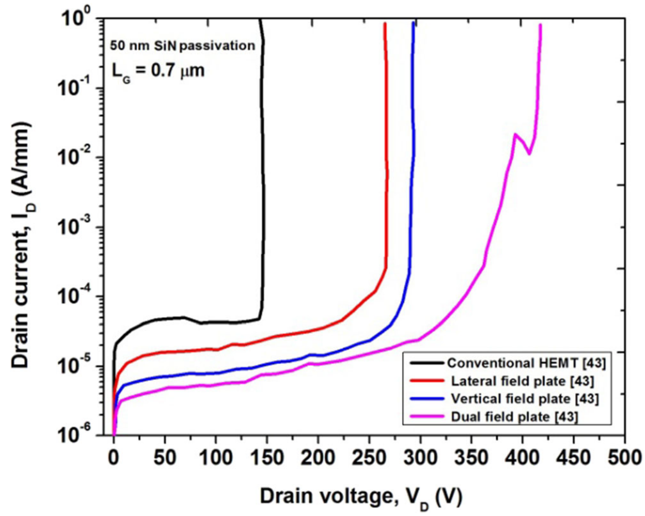


**Fig. 7** Drain connected field plate Breakdown characteristics [43]

The distributions of electric field along the $Al_{0.3}Ga_{0.7}N$ barrier of HEMTs are shown in Fig. 5. There is a peak electric field near the gate and FP edge forming two triangular lobes. It is observed that the breakdown field depends on the total area under these lobes. The higher the area for SiN passivation DH-HEMT leads to high breakdown voltage than other devices shown in Fig. 4.

Figures 6 and 7 shows the breakdown characteristics of gate field plate [42] and drain field plate [43] respectively. The proposed DH-HEMT with gate field plate HEMT in this works demonstrated a significant improvement in breakdown voltage than existing works.

The transfer characteristics of the proposed DH-HEMTs at $V_{DS} = 5$ V are depicted in Fig. 8. The HEMT with SiN passivation drain current reached 1.4 A/mm at zero gate voltage and the HEMT with $SiO_2$ passivation had shown 1.3 A/mm. The proposed DH-HEMT in this work had shown high current density than conventional HEMTs [27, 28, 30, and]. The high drain current achieved in the proposed work mainly because of high sheet charge density ($n_s$), high mobility, and low contact resistances.

The sub-threshold leakage current characteristics of HEMTs are depicted in Fig. 9. DH-HEMT with SiN passivation demonstrated a very low leakage current of ~$1 \times 10^{-13}$ A/mm than other devices. The $Al_{0.04}Ga_{0.96}N$ blocking layer helps the device in outstanding confinement of electrons towards the channel, resulting in suppressed sub-threshold current and hence improves the breakdown voltage. The back-barrier material is used in this work to reduce the buffer leakage effectively. The bulk punch-through under the depletion region is the major source of buffer leakage, which is reduced in the proposed device structure.

Figure 10 displays the transconductance ($G_M$) variation with $V_{GS}$. The $SiO_2$ passivation HEMT showed a peak $G_M$ of 550 mS/mm and SiN passivation HMTs showed 540 mS/mm.

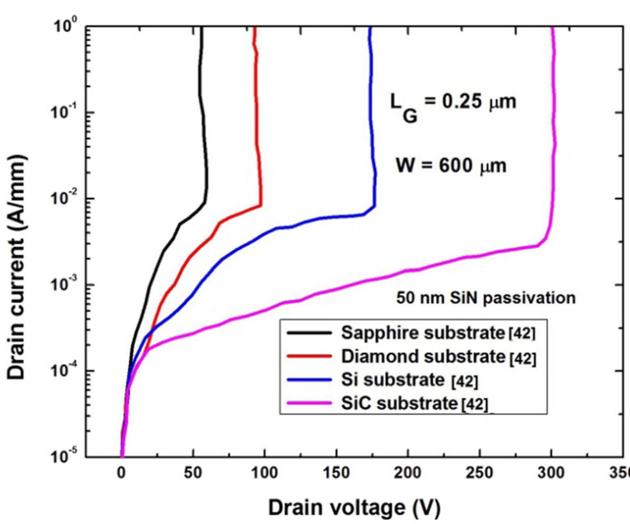


**Fig. 6** Gate field plate HEMTs breakdown characteristics [42]

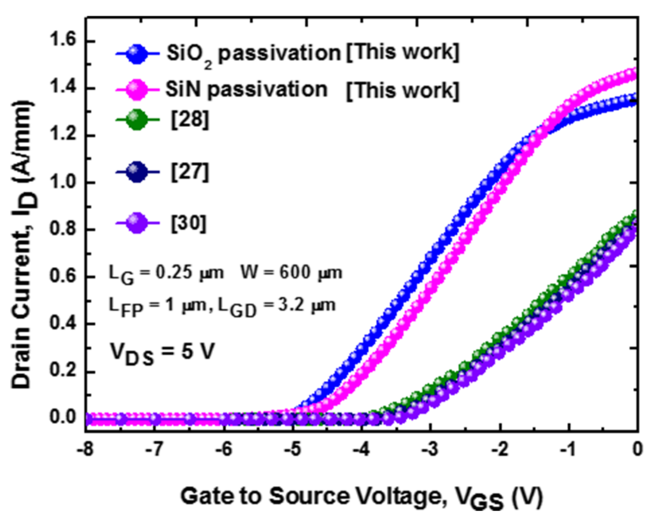


**Fig. 8** Transfer characteristics

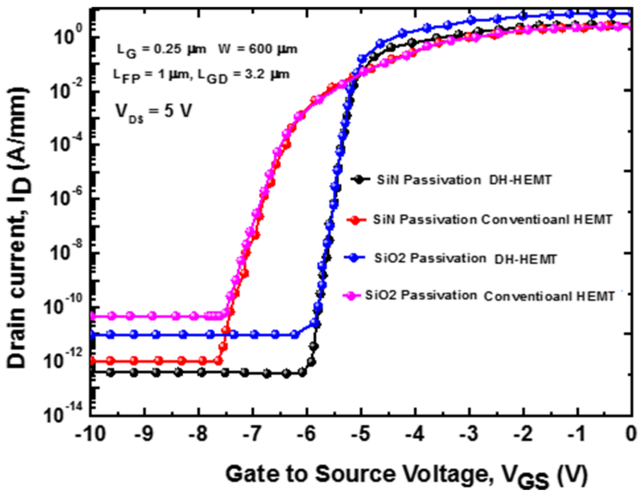


**Fig. 9** Sub-threshold current curves for SiN and $SiO_2$ passivation in proposed and conventional HEMTs

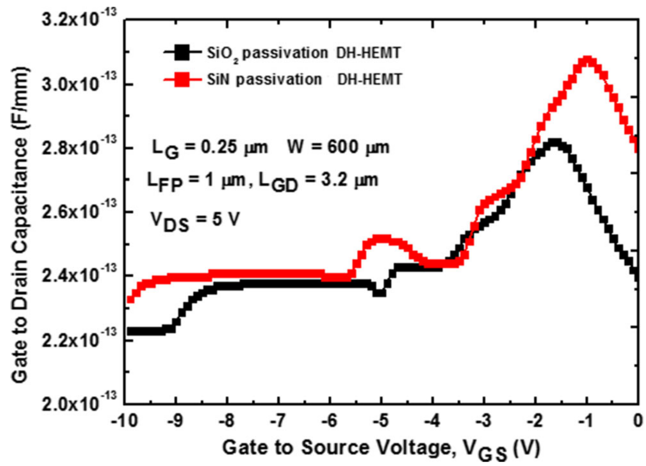


**Fig. 11** Gate to Drain capacitance ($C_{GD}$) characteristics

The $f_T$ and $f_{MAX}$ of the HEMTs are limited by the device's intrinsic capacitances ($C_{GS}$ and $C_{GD}$). The TCAD simulation is carried out for small-signal characteristics of proposed DH-HEMTs and plotted in Figs. 11 and 12. The $C_{GD}$ of HEMT with SiN ($SiO_2$) passivation is ~$2.4 \times 10^{-13}$ (~$2.35 \times 10^{-13}$) F/mm below the threshold voltage and rapidly decreasing with the $V_{GS}$ above threshold voltage and reached $2.8 \times 10^{-13}$ ($2.3 \times 10^{-13}$) F/mm at $V_{GS} = 0$ V shown in Fig. 11. The $C_{GS}$ value of proposed HEMT with SiN($SiO_2$) passivation is $2.3 \times 10^{-13}$ ($1.6 \times 10^{-13}$)F/mm at the off-sate condition and when the $V_{GS}$ reaches the threshold voltage of the device, the $C_{GS}$ started increasing sharply and reached $1.2 \times 10^{-12}$ ($5 \times 10^{-12}$) F/mm at $V_{GS} = 0$ V shown in Fig. 12. One of the key factors to enhance the high-gain millimeter-wave power amplification is the $f_{MAX}$ of the device which can be expressed as [31, 32];

$$f_{MAX} = \frac{f_T}{2\sqrt{(R_I + R_S + R_G)/(R_{DS} + (2\pi f_T)R_G C_{GD})}} \quad (6)$$

Where $R_G$, $R_{DS}$, $R_S$, $R_I$ are gate resistance, output resistance, source resistance, and gate charging resistance respectively.

The small-signal RF characteristics of the proposed DH-HEMTs at peak $g_m$ bias are shown in Fig. 13. The $f_T$ and $f_{MAX}$ of the DH-HEMT with SiN ($SiO_2$) passivation is extracted by using −20 dB/decade slopes of $|h_{21}|^2$ and $|U_g|$. The SiN ($SiO_2$) surface passivation DH-HEMT demonstrated an outstanding $f_T/f_{MAX}$ of 54/198 (62/252) GHz. The n + doped source and region in the proposed device reduces the contact resistances and the low permittivity passivation techniques improve the high frequency operation of the device. However, SiN passivation HEMT shows low $f_T/f_{MAX}$ than $SiO_2$ passivation device. This is mainly because of the permittivity of the SiN ($\varepsilon_{SiN} \sim 7.5$) is higher than the $SiO_2$ ($\varepsilon_i \sim 3.9$) results in high parasitic capacitance ($C = \frac{\varepsilon A}{d}$ ), which lowering the high frequency operation of the SiN passivation device.

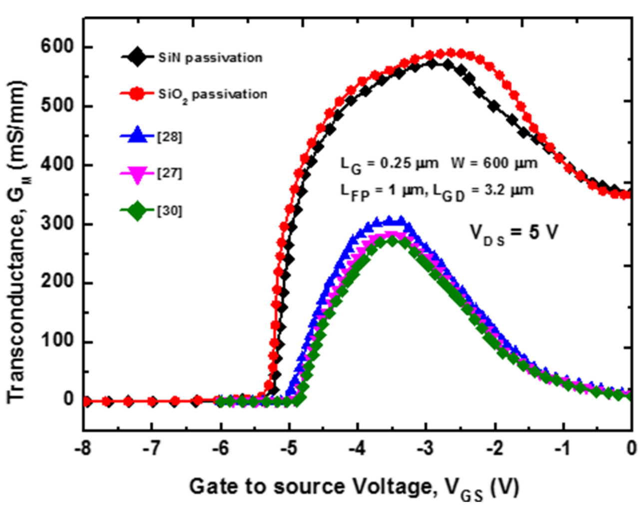


**Fig. 10** Transconductance characteristics

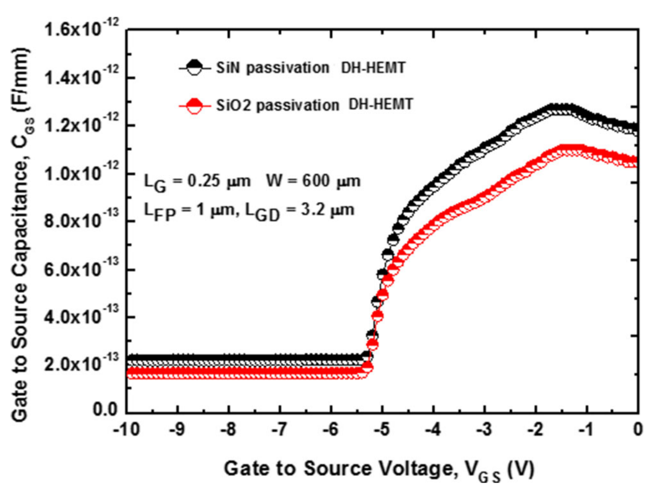


**Fig. 12** Gate to source capacitance ($C_{GS}$) characteristics

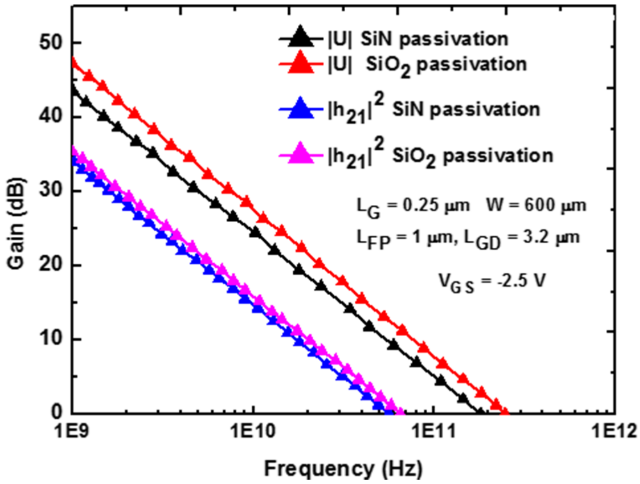


**Fig. 13** RF characteristics

The comparison of proposed HEMT performance with the state of the art of GaN-HEMTs are displayed in Table 2. The proposed gate field plate DH-HEMTs with thick passivation layers in this work had shown high breakdown voltage along with high $f_T/f_{MAX}$ than existing works. The operating frequency of the HEMT can be enhanced by further scaling of the device dimensions.

**Table 2** Comparison of proposed DH-HEMTs performance with the state of the art of GaN-HEMTs for high power microwave applications

| Reference, year | $L_G$ (µm) | $V_{BR}$ (V) | $f_T$ (GHz) | JFoM (THz-V) |
|---|---|---|---|---|
| [2], 2005 | 0.2 | 65 | 60 | 3.9 |
| [4], 2004 | 0.15 | 100 | – | – |
| [7], 2013 | 0.1 | 176 | 50 | 8.8 |
| [12], 2011 | 0.6 | 82 | 19 | 1.558 |
| [21], 2004 | 0.7 | 150 | 20 | 3 |
| [22], 2008 | 0.14 | 100 | 50 | 5 |
| [23], 2012 | 0.1 | 29 | 96 | 2.784 |
| [24], 2007 | 1 | 30 | 14.1 | 0.423 |
| [25], 2017 | 0.1 | 146 | 53 | 7.738 |
| [26], 2012 | 0.8 | 375 | – | – |
| [27], 2019 | 0.25 | 330 | 20.2 | 6.666 |
| [28], 2019 | 0.25 | 342 | 28 | 9.576 |
| [29], 2018 | 0.25 | 312 | – | – |
| [42], 2020 | 0.25 | 298 | 17.4 | 5.185 |
| [43], 2020 | 0.7 | 265 | 55 | 14.57 |
| [44], 2020 | 0.7 | 250 | – | – |
| This work (SiN Passivation) | 0.25 | 496 | 54 | 28.76 |
| This work ($SiO_2$ Passivation) | 0.25 | 292 | 62 | 19.27 |

## 4 Conclusion

A systematic study of gate field plate in combination with an $Al_{0.04}Ga_{0.96}N$ blocking layer and a 0.5 µm thick passivation ($SiN/SiO_2$) DH-HEMTs has been studied using TCAD. The introduction of $Al_{0.04}Ga_{0.96}N$ blocking layer enabled outstanding electron confinement in the channel, which leads to the reduction of sub-threshold leakage. The optimized gate field plate $Al_{0.3}Ga_{0.7}N/GaN/Al_{0.04}Ga_{0.96}N$ HEMT along with a thick passivation layer shown high breakdown voltage and high $f_T/f_{MAX}$. The proposed double heterojunction HEMT with SiN passivation showed a 40% improvement in breakdown voltage than $SiO_2$ passivation HEMT. The Johnson Figure of Merit (JFoM) along with excellent $f_{max} \times V_{br}$ product proves that the proposed DH-HEMTs with proper device optimizations are promising candidates for U and V band high power microwave wave applications.

**Author Contributions** All the works in this paper have done together by P. Murugapandiyan, D. Nirmal, J. Ajayan, Arathy Varghese and N. Ramkumar.

**Data Availability** Not applicable.

## Compliance with Ethical Standards

The authors declare that they have no known competing financial interests or personal relationships that could have appeared to influence the work reported in this paper.

**Conflict of Interest** The authors declare that there is no conflict of interest reported in this paper.

**Code Availability** Not applicable.

**Consent to Participate** Not applicable.

**Consent for Publication** Not applicable as the manuscript does not contain any data from individual.

## References

1. Ikeda N, Niiyama Y, Kambayashi H, Sato Y, Nomura T, Kato S, Yoshida S (2010) GaN power transistors on Si substrates for switching applications. Proc IEEE 98:1151–1161
2. Moon JS, Wu S, Milosavljevic I, Conway A, Hashomoto P, Hu M, Antcliffe M, Micovicv M (2005) Gate-recessed AlGaN-GaN HEMTs for high-performance millimeter-wave applications. IEEE Electron Device Lett. 26:348–350
3. Palacios T, Charkraborty A, Rajan S, Poblenz C, Keller S, DenBaars SP, Speck JS, Mishra UK (2005) High-power AlGaN/GaN HEMTs for Ka-band applications. IEEE Electron Device Lett. 26:781–783
4. Chu KK, Chao PC, Pizzella MT, Actis R, Meharry DE, Nichols KB, Vaudo RP, Xu X, Flynn JS, Dion J, Brandes GR (2004) 9.4 W/mm power density AlGaN-GaN HEMTs on free-standing GaN substrates. IEEE Electron Device Lett. 25:596–598

5. Vetury R, Zhang N, Keller S, Mishra U (2001) The impact of surface states on the DC and RF characteristics of AlGaN/GaN HFETs. IEEE Trans Electron Devices 48:560–566
6. Huang H, Liang YC, Samudra GS, Chang T-F, Huang C-F (2014) Effects of gate field plates on the surface state related current collapse in AlGaN/GaN HEMTs. IEEE Trans Power Electronics 29: 2164–2173
7. Brown DF, Shinohara K, Corrion AL, Chu R, Williams A, Wong JC, Alvarado-Rodriguez I, Grabar R, Johnson M, Butler CM, Santos D, Burnham SD, Robinson JF, Zehnder D, Kim SJ, Oh TC, Micovic M (2013) High-speed, enhancement-mode GaN power switch with regrown n+ GaN ohmic contacts and staircase field plates. IEEE Electron Device Lett. 34:1118–1120
8. Wu Y-F, Moore M, Saxler A, Wisleder T, Parikh P (2006) 40-W/mm double field-plated GaN HEMTs. in Proc IEEE Device Res Conf:151–152
9. Wakejima A, Ota K, Matsunaga K, Kuzuhara M (2003) A GaAs-based field-modulating plate HFET with improved WCDMA peak-output-power characteristics. IEEE Trans Electron Devices 50: 1983–1987
10. Pei Y, Chen Z, Brown D, Keller S, Denbaars SP, Mishra UK (2009) Deep-submicrometer AlGaN/GaN HEMTs with slant field plates. IEEE Electron Device Lett. 30:328–330
11. Coffie R (2014) Slant field plate model for field-effect transistors. IEEE Trans Electron Devices 61:2867–2872
12. Hao Y, Yang L, Ma X, Ma J, Cao M, Pan C, Wang C, Zhang J (2011) High-performance microwave gate-recessed AlGaN/AlN/GaN MOS-HEMT with 73% power-added efficiency. IEEE Electron Device Lett 32:626–628
13. Saito W, Nitta T, Kakiuchi Y, Saito Y, Tsuda K, Omura I, Yamaguchi M (2007) Suppression of dynamic ON-resistance increase and gate charge measurements in high-voltage GaN-HEMTs with optimized field-plate structure. IEEE Trans Electron Devices 54:1825–1830
14. Nidhi T, Palacios A, Chakraborty SK, Mishra UK (2006) Study of impact of access resistance on high-frequency performance of GaN HEMTs by measurements at low temperature. IEEE Electron Device Lett 27:877–880
15. Tasker PJ, Hughes B (1989) Importance of source and drain resistance to the maximum ft of millimeter-wave MODFETs. IEEE Electron Device Lett. 10:291–293
16. Bolognesi CR, Kwan AC, DiSanto DW (2002) Transistor delay analysis and effective channel velocity extraction in GaN HFETs. IEDM Tech Dig 4:685–688
17. Hanawa H, Horio K (2014) Increase in breakdown voltage of AlGaN/GaN HEMTs with a high-k dielectric layer. Phys Status Solidi A 211:784–787
18. Liu C, Chor EF, Tan LS (2007) Enhanced device performance of AlGaN/GaN HEMTs using $HfO_2$ high-k dielectric for surface passivation and gate oxide. Semicond Sci Technol 22:522–527
19. Micovic M, Hashimoto P, Hu M, Milosavljevic I, Duvall J, Willadsen PJ, Wong W-S, Conway AM, Kurdoghlian A, Deelman PW, Moon J-S, Schmitz A, Delaney MJ (2004) GaN double heterojunction field effect transistor for microwave and millimeterwave power applications. IEDM Tech Dig 4:807–810
20. ATLAS User's Manual, Device simulation software, (2009) SILVACO Int., Santa Clara, CA,
21. Chini A, Buttari D, Coffie R, Shen L, Heikman S, Chakraborty A, Keller S, Mishra UK (2004) Power and linearity characteristics of field-plated recessed-gate AlGaN–GaN HEMTs. IEEE Electron Device Lett 25:229–231
22. Moon JS, Wong D, Hu M, Hashimoto P, Antcliffe M, McGuire C, Micovic M, Willadson P (2008) 55% PAE and high power Ka-band GaN HEMTs with linearized Transconductance via n+ GaN source contact ledge. IEEE Electron Device Lett 29:834–837
23. Marti D, Tirelli S, Alt AR, Roberts J, Bolognesi CR (2012) 150-GHz cutoff frequencies and 2-W/mm output power at 40 GHz in a millimeter-wave AlGaN/GaN HEMT technology on silicon. IEEE Electron Device Lett 33:1372–1374
24. Song D, Liu J, Cheng Z, Tang WCW, Lau KM, Chen KJ (2007) Normally off AlGaN/GaN low-density drain HEMT (LDD-HEMT) with enhanced breakdown voltage and reduced current collapse. IEEE Electron Device Lett 28:189–191
25. Wong J, Shinohara K, Corrion AL, Brown DF, Carlos Z, Williams A, Tang Y, Robinson JF, Khalaf I, Fung H, Schmitz A, Thomas O, Kim S, Chen S, Burnham S, Margomenos A, Micovic M (2017) Novel asymmetric slant field plate Technology for High-Speed low-Dynamic Ron E/D-mode GaN HEMTs. IEEE Electron Device Lett 38:95–98
26. Xie G, Xu E, Lee J, Hashemi N, Zhang B, Fu FY, Ng WT (2012) Breakdown-voltage-enhancement technique for RF-based AlGaN/GaN HEMTs with a source-connected air-bridge field plate. IEEE Electron Device Lett 33:670–672
27. Fletcher A, Nirmal D, Ajayan J, Arivazhagan L (2019) Analysis of AlGaN/GaN HEMT using discrete field plate technique for high power and high frequency applications. Int J Electron Commun 99: 325–330
28. Augustine Fletcher AS, Nirmal D, Arivazhagan L, Ajayan J, Varghese A (2019) Enhancement of Johnson figure of merit in III-V HEMT combined with discrete field plate and AlGaN blocking layer. Int J RF Microw Comput Aided Eng 30:e22040
29. Chandera S, Guptaa S, Ajayb MG (2018) Enhancement of breakdown voltage in algan/gan hemt using passivation technique for microwave application. Superlattices and Microstructures 120: 217–222
30. Subramani NK, Julien C, Ahmad A, Jean C, Raphael S, Raymond Q (2017) Identification of GaN buffer traps in microwave power AlGaN/GaN HEMTs through low frequency S parameters measurements and TCAD-based physical device simulations. J Elect Dev Soc 5:12–18
31. Adachi S (2008) Properties of semiconductor alloys: group-IV, III-V and II-VI semiconductors. Wiley, Chichester
32. Giovanni C, Dongping X, Schreurs DM, Multibias A (2006) Equivalent-circuit extraction for GaN HEMTs. IEEE Trans Microwave Theory Tech 54:3616–3622
33. Kawada Y, Hanawa H, Horio K (2017) Effects of acceptors in a Fe-doped buffer layer on breakdown characteristics of AlGaN/GaN high electron mobility transistors with a high-*k* passivation layer. Jpn J Appl Phys 108003:1–3
34. Satoh Y, Hanawa H, Horio K (2016) Effects of buffer leakage current on breakdown voltage in AlGaN/GaN HEMTs with a high-k passivation layer, 2016 11th European Microwave Integrated Circuits Conference (EuMIC), London, 341-344,
35. Kabemura T, Ueda S, Kawada Y, Horio K (2018) Enhancement of breakdown voltage in AlGaN/GaN HEMTs: field plate plus high- *k* passivation layer and high acceptor density in buffer layer, in. IEEE Transactions on Electron Devices 65:3848–3854
36. Karmalkar S, Mishra UK (2001) Enhancement of breakdown voltage in AlGaN/GaN high electron mobility transistors using a field plate. in IEEE Transactions on Electron Devices 48:1515–1521
37. Brown DF (2013) High-speed, enhancement-mode GaN power switch with regrown n+ GaN Ohmic contacts and staircase field plates. IEEE Electron Device Letters 4:1118–1120
38. Saito W, Suwa T, Uchihara T, Naka T, Kobayashi T (2015) Breakdown behaviour of high-voltage GaN-HEMTs. Microelect Real 55:1682–1686
39. Meneghesso G, Meneghini M, Zanoni E (2014) Breakdown mechanisms in AlGaN/GaN HEMTs: an overview. Japan J App Phy 53: 1–9

40. Binola K, Shobha R, Prajoon P, Mohankumar N, Nirmal D (2015) The influence of high-k passivation layer on breakdown voltage of schottky AlGaN/GaN HEMTs. J Microelectron 46:1387–1391
41. Toshiki K, Shingo U, Yuki K, Kazushige H (2018) Enhancement of breakdown voltage in AlGaN/GaN HEMTs: field plate plus high-*k* passivation layer and high acceptor density in buffer layer. IEEE Trans Elect Dev 65:9–14
42. Fletcher ASA, Nirmal D, Ajayan J, Arivazhagan L (2020) An intensive study on assorted substrates suitable for high JFOM AlGaN/GaN HEMT. Silicon. https://doi.org/10.1007/s12633-020-00549-4
43. Soni A, Ajay, Shrivastava M (2020) Novel drain-connected field plate GaN HEMT designs for improved $V_{BD}$–$R_{ON}$ tradeoff and RF PA performance. IEEE Transactions on Electron Devices 67(4): 1718–1725. https://doi.org/10.1109/TED.2020.2976636
44. Prasannanjaneyulu B, Karmalkar S (2020) Relative effectiveness of high-*k* passivation and gate-connected field plate techniques in enhancing GaN HEMT breakdown. Microelectron Reliab 110: 113698. https://doi.org/10.1016/j.microrel.2020.113698